JOURNAL OF ADVANCED MECHANICAL ENGINEERING APPLICATIONS
e-ISSN: 2716-6201

JAMEA

Vol. 6 No. 1 (2025) 70-79
https://publisher.uthm.edu.my/ojs/index.php/jamea

CFD Analysis on the Effects of Various Train Lengths on Aerodynamic Loads and Flow Structure for Train Travelling Through Various Crosswind Conditions

Lai Swee Yong[1], Izuan Amin Ishak[1]*, Mohammad Arafat[1], Nurnida Elmira Othman[2] , Nur Haziqah Shaharuddin[3], Nurshafinaz Mohd Maruai[4]

[1] *Department of Mechanical Engineering Technology, Faculty of Engineering Technology, Universiti Tun Hussein Onn Malaysia (UTHM), 84600 Pagoh, Johor, MALAYSIA*
[2] *School of Mechanical Engineering, College of Engineering, Universiti Teknologi MARA, Shah Alam, 40450, Selangor, MALAYSIA*
[3] *Department of Mechanical Engineering, Keio University, Yokohama, JAPAN*
[4] *Department of Mechanical Precision Engineering, Malaysia-Japan International Institute of Technology (MJIIT), Universiti Teknologi Malaysia (UTM), Jalan Sultan Yahya Petra, 54100, Kuala Lumpur, MALAYSIA*

*Corresponding Author: izuan@uthm.edu.my
DOI: https://doi.org/10.30880/jamea.2025.06.01.006

Article Info

Received: 2 February 2025
Accepted: 17 April 2025
Available online: 30 June 2025

Keywords

aerodynamic characteristics, ANSYS fluent, crosswind, Computational Fluid Dynamics (CFD), flow structures, high-speed train

Abstract

To ensure that railroad vehicles operate safely in crosswind conditions, it is essential to take into account the aerodynamic contribution of train length. As a result, this study aims to investigate the effect of different lengths of the Next-Generation High-Speed Trains (NG-HST) model when traveling under various crosswind conditions in terms of aerodynamic loads and flow structure formation with a Computational Fluid Dynamics (CFD) technique known as Reynold-Averaged Navier Stokes (RANS) combined with the k-epsilon (k–ε) turbulence model. Based on the train model's height and speed, the Reynolds number used is 1.3 x 10^6. The two aerodynamic performance characteristics, aerodynamic loads and flow structure formation, were analyzed using different train lengths: Case 1 (1 middle coach), Case 2 (3 middle coaches), and Case 3 (5 middle coaches) and varied crosswind yaw angles: 0°, 15°, 30°, 45°, and 60°. The findings indicate that as the crosswind yaw angle and train model's length increase, more flow comes into contact with the train model's surface on the windward side, resulting in a huge area of the high-pressure region and low-pressure region on the windward and leeward sides, respectively. In addition, the side force coefficient increases for the 60° crosswind yaw angle by about 12% for Case 3 (train with 5 middle coaches) compared to Case 1 (1 middle coach). Therefore, it can be concluded that the longer the train, the more pronounced the aerodynamic forces under high crosswind conditions, which may negatively impact stability and operational safety.

1. Introduction

In crosswinds, a high-speed train is surrounded by a very complicated flow field that will increase aerodynamic loads on the train, considerably reducing running safety and raising the chance of an overturn. In the context of rail transit, the public's knowledge of safety hazards, notably vehicle crosswind stability, has improved

considerably [1]. When a train is traveling under strong crosswind conditions, the aerodynamic performance of trains deteriorates, and air drag, lift, and lateral forces borne by trains quickly increase, which has an influence on the lateral stability of trains and even leads to overturning the train [2], [3]. When analyzing the train's lateral stability (rolling over or overturning) in crosswinds, the side force, lift force, and rolling moment are crucial aerodynamic loads to consider [4], [5], [6], [7], [8]. Besides, the lengths of the high-speed trains will also have some impact on the aerodynamic performance of the trains, since the fluctuation in the drag force is only observed when the number of coaches is less than five [9].

Riccoa *et al*. [10] found that the pressure caused by a long train running through a tunnel was greater and lasted longer than the pressure caused by a shorter train in a moving model test. This was due to the large surface area of the long train's body making contact with the wind flow from the surrounding region. Furthermore, Mao *et al*. [11] also analyze the influence of train formation on the aerodynamic characteristics of high-speed trains under crosswind and find that although the number of cars has less influence on the drag force coefficient, lift force coefficient, lateral force coefficient, and overturning moment coefficient of the head car, it has a greater influence on those of the tail car. Many efforts have been undertaken to enhance the aerodynamic performance of high-speed trains; for instance, modifications to the streamlined head length or other train parts have been discovered to have an impact on the pressure waves that occur during train rendezvous, as well as lift and steady-state aerodynamic pressure on the train surface [12].

Some research has shown that lower drag coefficients were found for train models that were stretched in the center by adding additional carriages [13]. Therefore, there has been some research about the effect of a train's length on its aerodynamic performance that has been conducted. Chen *et al*. [14] analyzed the distribution region and intensity of velocity fluctuation with different train lengths and discussed the streamwise velocity, the pressure, the drag and lift coefficient, and the mean and instantaneous slipstream velocities with different train lengths. The study shows that the drag force coefficient increases by about 0.382 for case 3 compared to case 1. Additionally, longer trains exhibited increased velocity fluctuations and higher aerodynamic forces, which could compromise stability. They reported that slipstream effects intensified with train length, influencing drag and lift forces. Niu *et al*. [15] investigate the aerodynamic performance of trains of different lengths under a crosswind with or without a windbreak. The train's design directly influences its aerodynamic performance, which includes aerodynamic forces, slipstream, and wake flow, as the train's speed increases [16]. As the yaw angle of the crosswind increases, there might have been an incident of train overturning happening [17]. Based on the research of Arafat *et al*. [18], the result indicates that a larger yaw angle, which is primarily determined by the incoming wind velocity, can lead to higher flow separation and a more complex three-dimensional flow around the train. While previous studies have examined aerodynamic forces on high-speed trains under crosswind conditions, limited research has focused on the combined effects of train length and yaw angle on aerodynamic performance.

Therefore, this study focuses on investigating the aerodynamic performance of the Next-Generation High-Speed Train (NG-HST) of different lengths under a crosswind. In this study, computational fluid dynamics (CFD) combined with the unsteady Reynolds-averaged Navier-Stokes equation (URANS) will be applied as the numerical simulation.

2. Related Work

Fig. 1 shows the research flow chart of CFD analysis. In this research, the NG-HST train model is simplified for the computational train model, as shown in Fig. 2. Three lengths (13.33 *H*, 21.94 *H*, and 30.54 *H*) are used for the train model to study the effect of the length on the aerodynamic performance of the train. This represents the three types of train models with case 1, case 2, and case 3, as shown in Fig. 2(a). The width (*W*) and height (*H*) of the computational train model are 0.122 m and 0.186 m, as shown in Fig. 2(b).

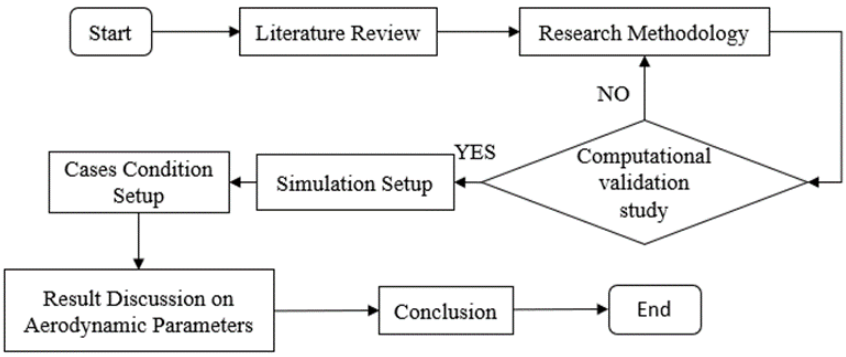

Fig. 1 *Research flow chart*

J. of Advanced Mechanical Engineering Applications Vol. 6 No. 1 (2025) p. 70-79

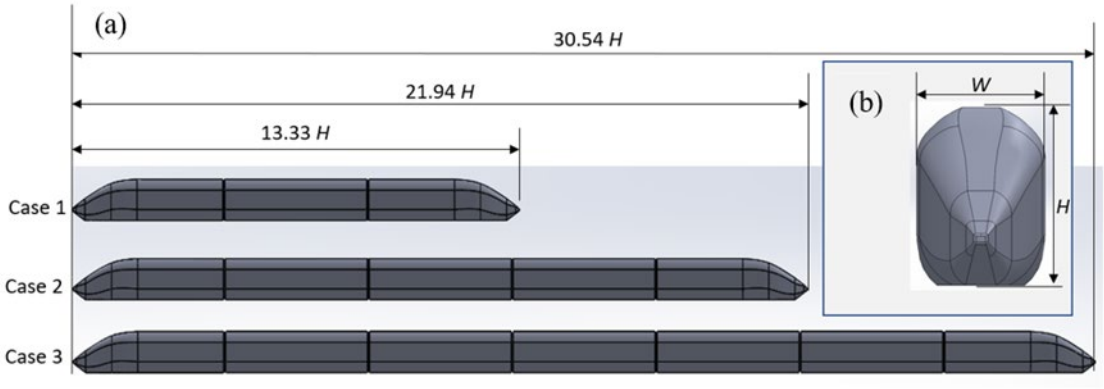

Fig. 2 *Train model: (a) different lengths of the train; (b) train cross-section*

Based on available wind tunnel data, a length of 7.74 H, consisting of the front coach and a half section of the middle coach, was used for validation. Then, the computational validation study will proceed with the grid independence study and validation with previous research. After obtaining the validation study results, the simulation setup proceeded with the *k*-epsilon (*k*–*ε*) turbulence model and Reynolds number of 1.3 x 10^6 for three cases, which were cases 1, 2, and 3, and different crosswind yaw angles, which were 0°, 15°, 30°, 45°, and 60°. The yaw angles were chosen to cover common crosswind scenarios encountered by high-speed trains, ensuring a comprehensive aerodynamic assessment. The Reynolds number was used to determine whether the flow of fluid was laminar or turbulent [19]. Further, the simulation proceeds with case condition setup, and each of the cases will be tested under different crosswind yaw angles. Finally, the discussion and conclusion will be given for the analysis of the effect of aerodynamic loads and flow structure formation around the train with different lengths under different crosswind conditions.

3. Methodology

a. Boundary Conditions

The computational domain must be discretized into a computational grid in order to solve the discretized equations of fluid flows (or mesh). Fig. 3 shows the enclosure condition for the computational domain, following Ref. [20], ensuring that boundary effects were minimized. There is a gap between the train model and the ground surface, and the distance between them is 0.025 m (distance between the upper surface of the track and the bottom surface of the train, as shown in Fig. 3(b). The distance between the train model and the back is 3 m, while the distance between the train model and the front is 1.5 m. The distance between the train model and the side is also 1.5 m, as shown in Fig. 3(a). These dimensions ensured sufficient space for flow development and vortex dissipation. The boundary condition of the models includes elements such as velocity inlet boundary, pressure outlet boundary, and symmetry boundaries, as shown in Fig. 4. The velocity inlet and pressure outlet boundaries were applied to the surface of the enclosure. The arrows in Fig. 4 indicate the boundary surfaces and do not represent flow direction. This setup ensured proper flow development without artificial constraints.

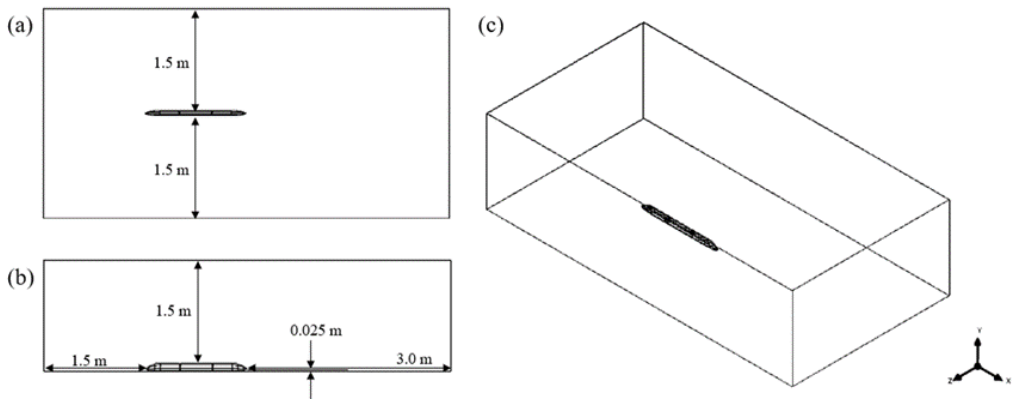

Fig. 3 *(a) size of the enclosure from the top view; (b) size of the enclosure from the side view; (c) isometric view of the enclosure*

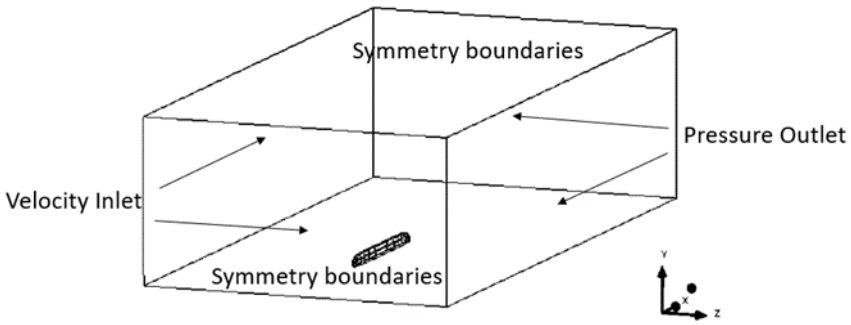

Fig. 4 *Boundary conditions*

b. Mesh Technique

Meshing is the method of discretizing a model into several elements [21], and the mesh efficiency can help to determine the accuracy of the results [22], [23]. The mesh generation employed a polyhedral meshing technique, which offers enhanced accuracy for complex geometries. The meshing parameter with coarse, medium, and fine mesh conditions and meshing structure conditions for the validation study have been shown in Table 1 and Fig. 5, respectively.

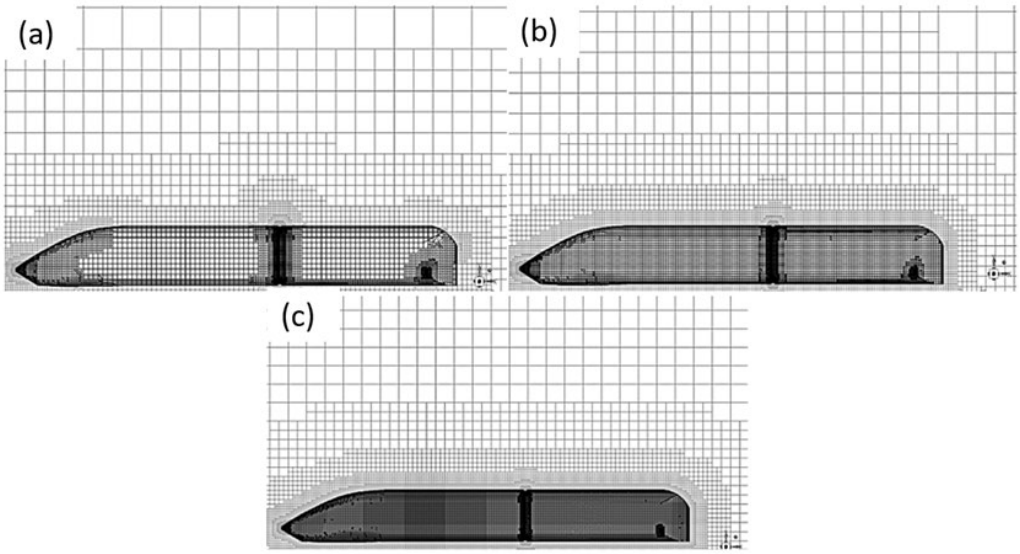

Fig. 5 *Meshing conditions: (a) Coarse; (b) Medium; (c) Fine*

Table 1 *Meshing parameter*

Cases	Element size (mm)	Face size (mm)	Affected diameter (mm)	Total nodes	Total element mesh
Coarse	256.0	20.0	2.0	276,932	234,049
Medium	128.0	7.0	8.0	364,767	314,284
Fine	64.0	4.0	12.0	775,713	688,740

c. Grid Independent Test

The CFD results based on the ANSYS software for the validation study are validated through the drag force coefficient (C_d) obtained from the simulation of different meshes. In addition, the simulation results were compared with experimental data from [24], showing good agreement in terms of aerodynamic force coefficients, confirming the reliability of the numerical approach. The results of C_d for the current research and previous research [24] for the different cases of mesh resolutions are presented in Table 2. Since the differences between the medium mesh case and experimental mesh case are not more than 1.0 %, it indicates that the medium mesh case with a C_d of 0.182 and the number of nodes of 364,767 is the most suitable for the validation of the study. The

medium and fine mesh showed a difference of 0.028%, well below the commonly accepted 1% threshold for engineering applications [25]. While adopting a 0.001% threshold for highly sensitive cases, such as biomedical and aerospace, our analysis demonstrated that further refinement beyond the fine mesh led to negligible changes, validating the mesh selection.

Table 2 *Drag force coefficient (C_d) for the current research and previous research with train models in different cases*

Cases	C_d
Coarse	0.188
Medium	0.182
Fine	0.182
Experimental	0.180

4. Results and Discussion

The results and discussion section presents data and analysis of the study for the quantitative and qualitative aerodynamics results, such as aerodynamic loads and flow structure around the train model. Quantitative results include the coefficients of aerodynamic forces such as drag (C_d), lift (C_l), side (C_s), rolling moment (C_{RL}), yawing moment (C_{YA}), and pitching moment (C_{PI}). Qualitative results include the streamline superimposed on the pressure contour and vortex core surrounding the train model.

a. Quantitative Results

Fig. 6 shows the results of the comparison of drag force (C_d), lift force (C_l), and side force coefficient (C_s) with respect to different lengths of NG-HST models when traveling under various crosswind conditions. From the results of the C_d, it shows that the overall trend for the C_d value for Cases 1, 2, and 3 was decreasing as the yaw angle increased from $\Psi = 0°$ until $\Psi = 60°$. Besides that, the absolute percentage differences between $\Psi = 0°$ and $\Psi = 60°$ for the C_d value of Cases 1, 2, and 3 were 81.21%, 72.91%, and 69.74%, respectively (Fig. 6a). From the comparison of the C_l, it shows that the overall trend for the C_l value of Cases 1, 2, and 3 was increasing as the yaw angles increased from $\Psi = 0°$ until $\Psi = 60°$. Besides that, the absolute percentage differences between $\Psi = 0°$ and $\Psi = 60°$ for the C_l value of Cases 1, 2, and 3 were 930.55%, 1470.73%, and 2047.08%, respectively (Fig. 6b). The comparison of the C_s shows that the C_s value of Cases 1, 2, and 3 was increasing as the yaw angle was increased from $\Psi = 0°$ until $\Psi = 60°$. The absolute percentage differences between $\Psi = 0°$ and $\Psi = 60°$ for the C_s value of Cases 1, 2, and 3 were 1323.57%, 1935.89%, and 2550.76%, respectively (Fig. 6c). Therefore, the result indicates that Case 3 has the worst results since the C_d, C_l, and C_s values were higher compared to Cases 1 and 2. Similar results in terms of drag force coefficients can be found in reference [14]. It is notable that the negative values in Fig. 6 and Fig. 7 indicate flow reversal, which occurs due to vortex shedding in the wake region. This phenomenon is commonly observed at high yaw angles and contributes to unsteady aerodynamic forces.

Next, Fig. 7 shows the results of the comparison of the rolling moment (C_{RL}), yawing moment (C_{YA}), and pitching moment (C_{PI}) with respect to different lengths of NG-HST models when travelling under various crosswind conditions. From the results of the C_{RL}, it shows that the overall trend for the C_{RL} value for cases 1, 2, and 3 decreased as the yaw angle increased from $\Psi = 0°$ until $\Psi = 60°$. Besides that, the absolute percentage differences between $\Psi = 0°$ and $\Psi = 60°$ for the C_{RL} value of Cases 1, 2, and 3 were 165.97%, 52.72%, and 73.83%, respectively. From the comparison of C_{YA}, it shows that the overall trend for the C_{YA} value of Cases 1, 2, and 3 was increasing as the yaw angles increased from $\Psi = 0°$ until $\Psi = 60°$. Besides that, the absolute percentage differences between $\Psi = 0°$ and $\Psi = 60°$ for the C_{YA} value of Cases 1, 2, and 3 were 2658.70%, 1156.13%, and 1856.02%, respectively. The comparison of the C_{PI} shows that the overall trend for the C_{PI} value of cases 1, 2, and 3 was decreasing as the yaw angle was increasing from $\Psi = 0°$ until $\Psi = 60°$. However, the trend pattern of the C_{PI} value of Case 3 fluctuated as shown in Fig. 7. The absolute percentage differences between $\Psi = 0°$ and $\Psi = 60°$ for the C_{PI} value of Cases 1, 2, and 3 were 645.41%, 313.00%, and 580.72%. Thus, it demonstrates that only the C_{RL}, C_{YA}, and C_{PI} were impacted by a crosswind on the train model for Case 2.

Relatively, in terms of aerodynamic loads, each of the cases obtained different results of aerodynamic load parameters. However, the trend pattern for the results for each of the cases was similar. For the Case 1 condition, the C_d, C_l, C_s, C_{RL}, and C_{PI} values were lower compared to Cases 2 and 3, while the C_{YA} value was higher compared to Cases 2 and 3. This demonstrates that the impact of crosswind on the aerodynamic load characteristics of the train model of Case 1 was minor. Moreover, for the condition of Case 2, the C_{RL} and C_{PI} values were higher compared to Cases 1 and 3, while the C_{YA} value was higher compared to Cases 1 and 3. It demonstrates that only the C_{RL}, C_{YA}, and C_{PI} were impacted by a crosswind on the train model for Case 2. Furthermore, for the Case 3 condition, the C_d, C_l, and C_s values were higher compared to Cases 2 and 3. In general, there will be more impact of

crosswind on the aerodynamic load characteristics on the train model of Case 3 due to more surface contact with the crosswind at the windward side of the train model as the crosswind yaw angle increases.

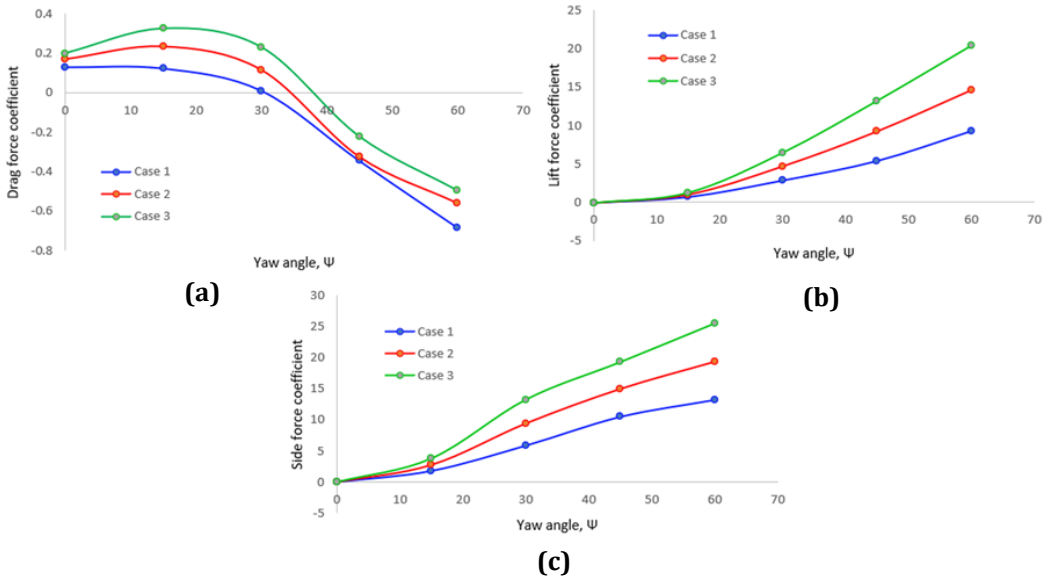

Fig. 6 *Comparison of the (a) drag force (C_d); (b) lift force (C_l); and (c) side force coefficient (C_s) with respect to different lengths of NG-HST models when travelling under various crosswind conditions*

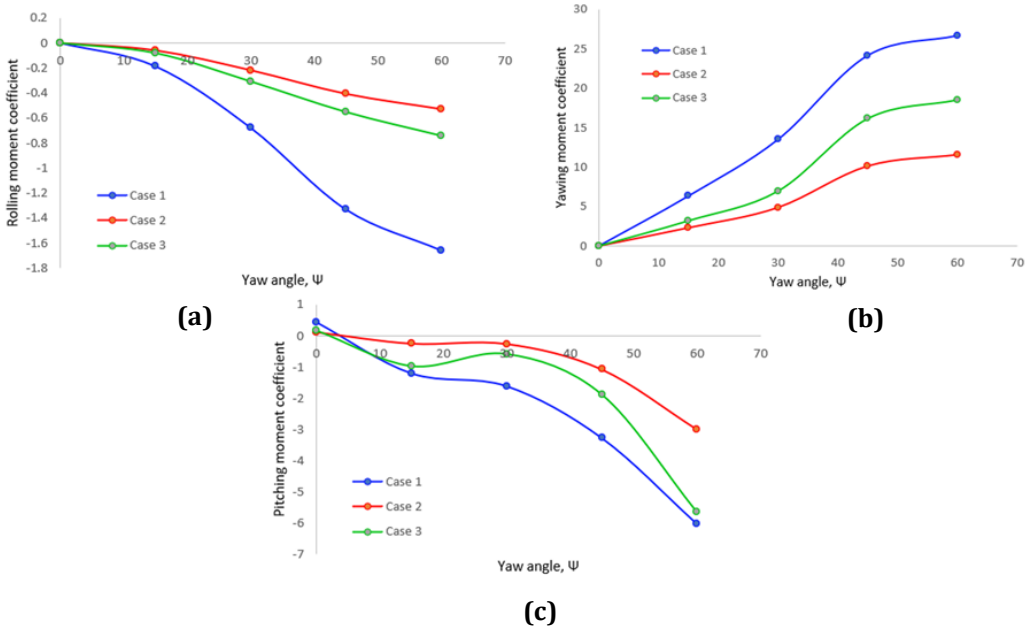

Fig. 7 *Comparison of the (a) rolling moment; (C_{RL}), (b) yawing moment (C_{YA}); and (c) pitching moment coefficient (C_{PI}) with respect to different lengths of NG-HST models when travelling under various crosswind conditions*

b. Qualitative Results

Fig. 8 shows the top view of the streamline flowing through the train model from the left side of the train model. It shows that the region of the high-pressure contour on the windward side and the low-pressure contour on the leeward side was expanding as the crosswind angle increased. The expansion of the low-pressure region suggests an increase in aerodynamic drag and side forces, which could negatively impact the train's stability. Previous studies [26] have shown that these pressure variations play a crucial role in determining side force coefficients, which influence train overturning moments under crosswind conditions. Fig. 9 shows the planes 1, 2, and 3 created at the midpoint of the middle car of the train model for cases 1, 2, and 3, respectively, and the streamline flow through the midpoint of the middle car from the left side of the train model. As the flow hit the windward surface of the train model, the flow was separated into two directions, which were towards the roof surface and

J. of Advanced Mechanical Engineering Applications Vol. 6 No. 1 (2025) p. 70-79

the bottom surface of the train model. A vortex was produced as the result of the flow separation at the leeward side of the middle car of the train model. For all the cases, it is similar that the number of vortices produced increased as the crosswind angle increased. At the same time, the radius of the vortex was also increasing as the crosswind angle increased. Besides that, the radius of the vortex near the rear car of the trained model was smaller than the radius of the vortex far away from the rear car of the train model. As the crosswind angle increased, the area of low-pressure contour was increasing at the leeward side of the midpoint of the middle car of the train model for each of the cases.

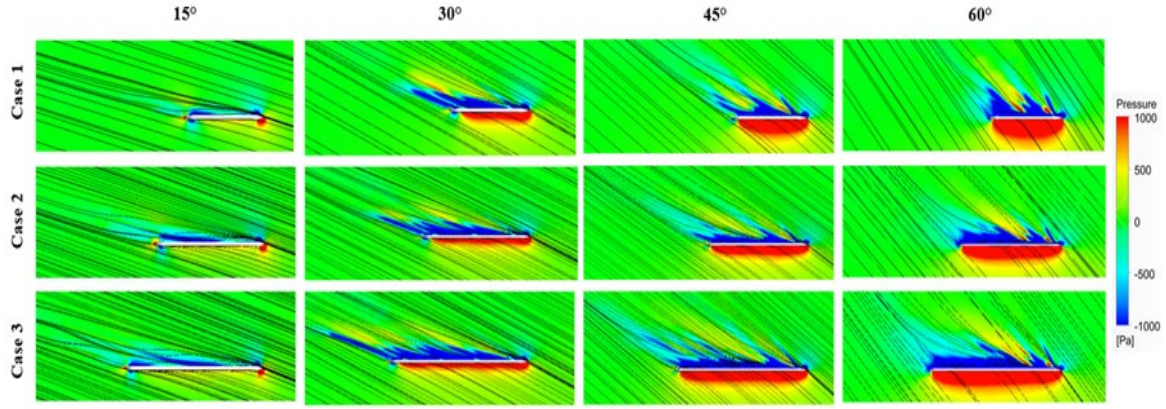

Fig. 8 *Streamlines superimposed on the pressure contour for different lengths of the NG-HST models from the top view under different crosswind angles*

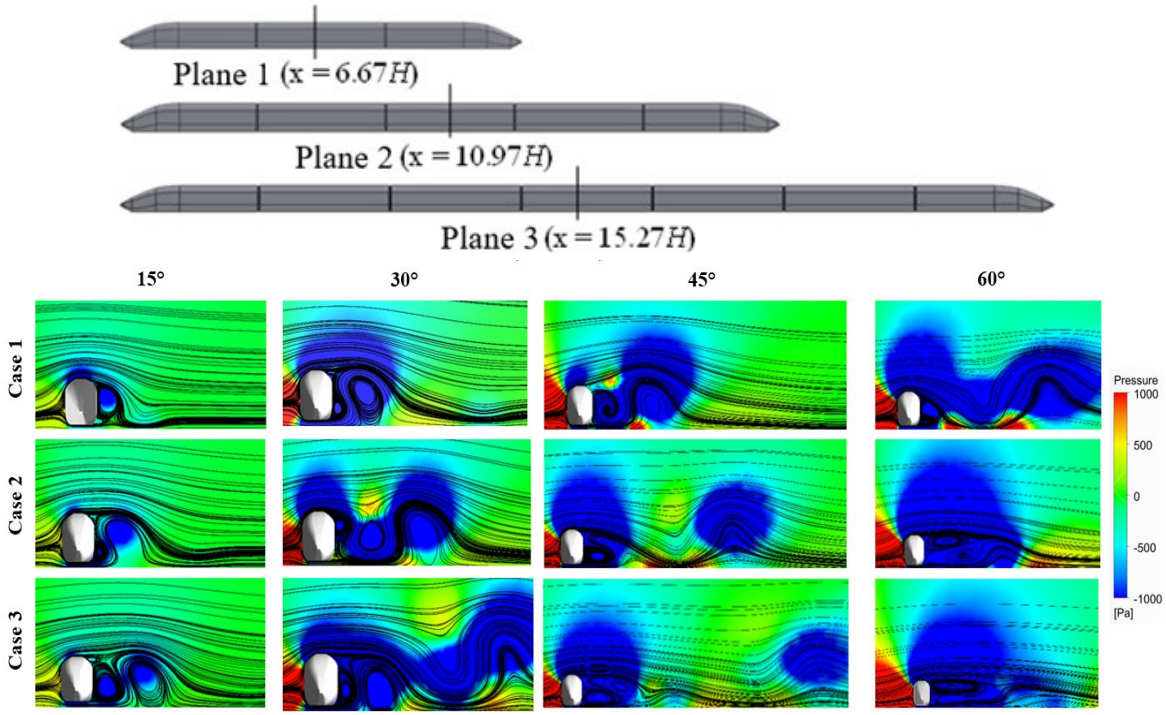

Fig. 9 *Planes created at the midpoint of the middle car of the trains: Plane 1 = 6.67 H, Plane 2 = 10.97 H, and Plane 3 = 15.27 H, and streamlines are superimposed on the pressure contour from the front view under different crosswind angles*

Fig. 10 illustrates the vortex core structures for different train lengths under varying crosswind angles. The results show that the vortex generation at the leeward side increased as the crosswind yaw angle increased, leading to stronger wake interactions. This phenomenon is primarily attributed to the increased pressure difference between the windward and leeward sides, which intensifies flow separation. Additionally, the vortex structures moved further away from the train body as the crosswind angle increased, indicating enhanced wake expansion. Furthermore, the number of vortices also increased with the train length. This is due to the larger surface area exposed to the crosswind on the windward side, resulting in stronger shear layers and more pronounced vortex formation. In Case 3, the longest train configuration, the highest number of vortices was

observed. This aligns with findings from previous studies [15], which demonstrated that longer vehicles experience more complex wake structures due to prolonged boundary layer development and flow detachment along their length. In addition, the increase in vortex formation at higher yaw angles can have both positive and negative effects. While vortex shedding contributes to aerodynamic instability, it also plays a role in pressure redistribution, which can mitigate side force imbalances [27]. However, excessive vortex generation, particularly in longer train models, can lead to stronger wake-induced unsteady forces, potentially compromising train stability and passenger comfort.

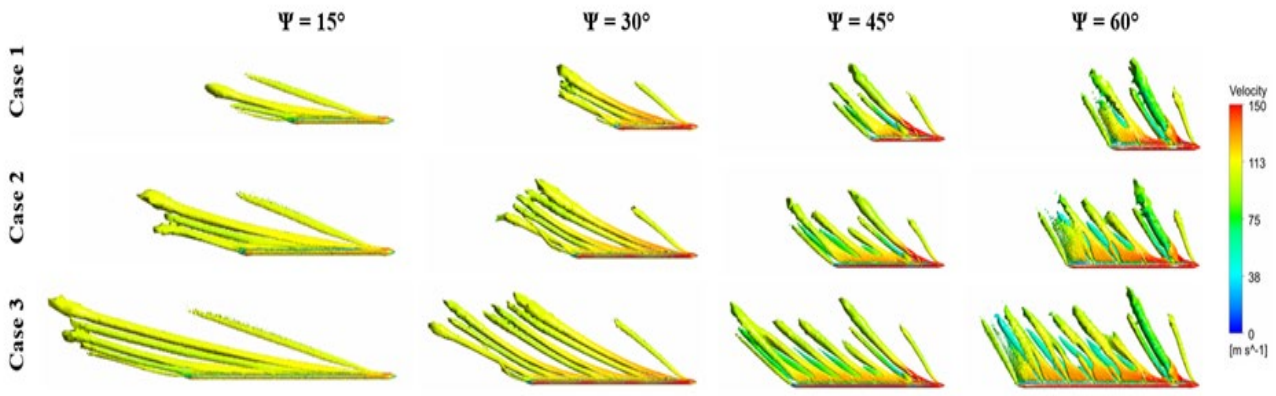

Fig. 10 *Vortex core for different lengths of the NG-HST models under different crosswind angles*

5. Conclusion

This study was conducted to analyze the effect of different lengths of NG-HST when travelling under various crosswind conditions in terms of aerodynamic loads and flow structure formations. In terms of the aerodynamic loads, the crosswind yaw angles have a significant impact. The lift force coefficient (C_l) and side force coefficient (C_s), two crucial factors that had a significant impact on the train's stability, revealed that Case 3 gave the worst results of these parameters when compared to Case 1 and Case 2. Two of the aerodynamic loads were critical and reached high values at high crosswind yaw angles (Ψ = 60º). According to the results of the current study at Ψ = 60º, Case 3 had the worst outcomes, followed by Case 2 and then Case 1.

In terms of flow structure formation, there were dissimilarities among the cases simulated for various crosswind conditions. Due to the different cases of the train model, the main difference was the number of vortices on the leeward side of the train model under crosswind conditions. As the crosswind yaw angle and the train model's length increase, there will be more surface contact with the crosswind on the train model's windward side, increasing the number of vortices.

Lastly, the last differences due to the different cases of the train model were the high-pressure region on the windward side and the low-pressure region on the leeward side of the train model under crosswind conditions. For Case 3, it consists of a large area of the high-pressure region on the windward side and a large area of a low-pressure region on the leeward side of the train model compared with Cases 1 and 2 at Ψ = 60º. This was due to the high crosswind yaw angle and longer lengths of the train model, which caused more flow to come into contact with the train model's surface on the windward side, which is why there was a large area of high-pressure and low-pressure regions in the train model's windward side and leeward side. This can cause the train to overturn due to the unbalanced pressure area on the train's leeward and windward sides. Therefore, it can be concluded that the longer the length of the train under high crosswind conditions, the greater the influence of the aerodynamic performance on the train

Acknowledgement

Communication of this research is made possible through monetary assistance by Universiti Tun Hussein Onn Malaysia.

Author Contribution

The authors confirm their contribution to the paper as follows: ***study conception and design:*** *Lai Swee Yong, Izuan Amin Bin Ishak, Mohammad Arafat;* ***data collection:*** *Lai Swee Yong;* ***analysis and interpretation of results:*** *Lai Swee Yong, Izuan Amin Bin Ishak, Mohammad Arafat;* ***draft manuscript preparation:*** *Lai Swee Yong, Izuan Amin Bin Ishak. All authors reviewed the results and approved the final version of the manuscript.*

References

[1] Guo, W. H., Xu, Y. L., & Asce, M. (2006). Safety Analysis of Moving Road Vehicles on a Long Bridge under Crosswind. *J Eng Mech*, vol. 132, no. 4, pp. 438–446. https://doi.org/10.1061/ASCE0733-93992006132:4438

[2] Grm, A., & Batista, M. (2017). Vehicle aerodynamic stability analysis under high crosswinds. *Strojniski Vestnik/Journal of Mechanical Engineering*, *63*(3), 191–200. https://doi.org/10.5545/sv-jme.2016.4095

[3] Huang, T., Li, S., Wan, Z., & Gu, Z. (2019). Investigation of vehicle stability under crosswind conditions based on coupling methods. *Proceedings of the Institution of Mechanical Engineers, Part D: Journal of Automobile Engineering*, *233*(13), 3305–3317. https://doi.org/10.1177/0954407018822424

[4] Sima, M., Eichinger, S., Blanco, A., & Ali, I. (2015). Computational fluid dynamics simulation of rail vehicles in crosswind: Application in norms and standards. *Proceedings of the Institution of Mechanical Engineers, Part F: Journal of Rail and Rapid Transit*, *229*(6), 635–643. https://doi.org/10.1177/0954409714551013

[5] Lin Ma, Xin Chen, Jun Wu, & Wanshui Han. (2018). Aerodynamic Interference Mechanism of Moving Vehicles on a Bridge Deck in Crosswind Environment. *Journal of Bridge Engineering*, 23(4). https://doi.org/10.1061/(ASCE)BE.1943-5592.0001194

[6] Charuvisit, S., Kimura, K., & Fujino, Y. (2004). Experimental and semi-analytical studies on the aerodynamic forces acting on a vehicle passing through the wake of a bridge tower in crosswind. *Journal of Wind Engineering and Industrial Aerodynamics*, *92*(9), 749–780. https://doi.org/10.1016/j.jweia.2004.04.001

[7] Fintelman, D., Hemida, H., Sterling, M., & Li, F. X. (2015). A numerical investigation of the flow around a motorbike when subjected to crosswinds. *Engineering Applications of Computational Fluid Mechanics*, *9*(1), 528–542. https://doi.org/10.1080/19942060.2015.1071524

[8] Arafat, M., Rajendran, S., Ishak, I. A., Al, M., & Zin, A. M. (2024). Effects of Crosswinds on The Flow Structure Around a Next-Generation High-Speed Train Exiting a Tunnel. *Jurnal Teknologi*, *86*(6), 29–37. https://doi.org/10.11113/jurnalteknologi.v86.20475

[9] Liu, L., Sun, Y., Chi, X., Du, G., & Wang, M. (2017). Transient aerodynamic characteristics of vans overtaking in crosswinds. *Journal of Wind Engineering and Industrial Aerodynamics*, *170*, 46–55. https://doi.org/10.1016/j.jweia.2017.07.014

[10] Chen, M.-K. (n.d.). *Use of a Rolling Road System in Crosswind Conditions*. Doctor of Philosophy (PhD), Dissertation, Mechanical & Aerospace Engineering, Old Dominion University. https://doi.org/10.25777/vng1-yf84

[11] Yudianto, A., Sofyan, H., Gunadi, & Fauzi, N. A. (2022). Aerodynamic Characteristics of Overtaking Bus under Crosswind: CFD Investigation. *CFD Letters*, *14*(8), 20–32. https://doi.org/10.37934/cfdl.14.8.2032

[12] Hammad, A., Xing, T., Abdel-Rahim, A., Durgesh, V., & Crepeau, J. C. (2019). Effect of Crosswinds on The Aerodynamics of Two Passenger Cars Crossing Each Other. *International Journal of Automotive Technology*, *20*(5), 997–1008. https://doi.org/10.1007/s12239-019-0094-8

[13] Noger, C., & van Grevenynghe, E. (2011). On the transient aerodynamic forces induced on heavy and light vehicles in overtaking processes. In *Int. J. Aerodynamics,* Vol. 1, No. 3-4, pp. 373-383. https://doi.org/10.1504/IJAD.2011.038851

[14] Corin, R. J., He, L., & Dominy, R. G. (2008). A CFD investigation into the transient aerodynamic forces on overtaking road vehicle models. *Journal of Wind Engineering and Industrial Aerodynamics*, *96*(8–9), 1390–1411. https://doi.org/10.1016/j.jweia.2008.03.006

[15] Uddin, M., Chellaram, A. D., & Robinson, A. C. (2017). CFD investigations of the aerodynamics of vehicle overtaking maneuvers. *AIP Conference Proceedings*, *1851*. https://doi.org/10.1063/1.4984714

[16] Alonso-Estébanez, A., del Coz Díaz, J., Álvarez Rabanal, F., Pascual, P., & García Nieto, P. (2018). Numerical investigation of truck aerodynamics on several classes of infrastructures. *Wind and Structures*, 26(1), pp. 35-43. https://doi.org/10.12989/was.2018.26.1.035

[17] Khairullah, N. N. A. A. N., Ishak, I. A., Arafat, M., Maruai, N. M., Sakri, F. M., & Khalid, A. (2024). Numerical Analysis on the Aerodynamic Performance of a High-speed Train Operating on Various Embankment Heights Under the Influence of Crosswinds. *International Journal of Integrated Engineering*, *16*(5), 34–45. https://doi.org/10.30880/ijie.2024.16.05.004

[18] Carsguide Autotrader Media Solutions Pty Ltd, "Nissan X-TRAIL Dimensions 2022," 2022. [Online]. Available: https://www.carsguide.com.au/nissan/x-trail/car-dimensions/2022

[19] Hou Man, Liu Bo, Peng Yun Dong, Chang Chung Man (2018). Design of Main Bridge of Second Penang Bridge in Malaysia. *International Journal of Transportation Engineering and Technology*, 4(2), pp. 35-42. https://doi.org/10.11648/j.ijtet.20180402.13

[20] Kamal, Muhammad Nabil Farhan, Izuan Amin Ishak, Nofrizalidris Darlis, Daniel Syafiq Baharol Maji, Safra Liyana Sukiman, Razlin Abd Rashid, and Muhamad Asri Azizul (2021). A review of aerodynamics influence on various car model geometry through CFD techniques. *Journal of Advanced Research in Fluid Mechanics and Thermal Sciences,* 88(1), pp. 109-125. http://doi.org/10.37934/arfmts.88.1.109125

[21] Hosain, M. L., & Fdhila, R. B. (2015). Literature Review of Accelerated CFD Simulation Methods Towards Online Application. Energy Procedia, 75, 3307–3314. https://doi.org/10.1016/j.egypro.2015.07.714.

[22] Francis H. Harlow, J Eddie Welch (1965). Numerical Calculation of Time-Dependent Viscous Incompressible Flow of Fluid with Free Surface. *The Physics of Fluids*, 8(12), 2182-2189. https://doi.org/10.1063/1.1761178

[23] Wu, Chengjun, Jiang Liu, and Jie Pan (2014). Influence of surrounding structures upon the aerodynamic and acoustic performance of the outdoor unit of a split air conditioner. *Chinese Journal of Mechanical Engineering,* 27(4), 836-845. http://doi.org/10.3901/CJME.2014.0515.095

[24] Abe, Masato, and Manning, W. (2009). Vehicle dynamics and control. *Vehicle Handling Dynamics*. 1-3. http://doi.org/10.1016/B978-1-85617-749-8.00001-5

[25] Favre, Tristan, and Gunilla Efraimsson. (2011). An assessment of detached-eddy simulations of unsteady crosswind aerodynamics of road vehicles. *Flow, Turbulence and Combustion,* 87, 133-163. http://doi.org/10.1007/s10494-011-9333-4

[26] Vasilopoulos, Konstantinos, Ioannis E. Sarris, and Panagiotis Tsoutsanis (2019). Assessment of airflow distribution and hazardous release dispersion around a single obstacle using Reynolds-averaged Navier-Stokes equations. *Heliyon*, 5(4). http://doi.org/10.1016/j.heliyon.2019.e01482

[27] Arafat, M., Ishak, I. A., Abdul Aziz, M. A. S., Soh, A. W. S., Tiong, W. T., Roziman, N. R., Mohd Hairul, N. A., Ramli, M. A., Ahmad Puaat, Z. M., Shahmuddin, S. H., & Abd Rashid, R. (2024). A Hybrid RANS/LES Model for Predicting the Aerodynamics of Small City Vehicles. *Journal of Advanced Research in Experimental Fluid Mechanics and Heat Transfer*, 17(1), 1–13. https://doi.org/10.37934/arefmht.17.1.113

[28] Chamkha, Ali J., and Younes Menni (2020). Hydrogen Flow over a Detached V-Shaped Rib in a Rectangular Channel. *Mathematical Modelling of Engineering Problems*, 7(2). http://doi.org/10.18280/mmep.070202

[29] Arafat, M., Amin Ishak, I., Mohd Maruai, N., Rusydi, M., Razif, M., Sakri, F. M., & Anugraha, R. A. (2025). CFD Letters CFD Assessment for Small UAV Propeller Aerodynamics. *CFD Letters*, *17*, 81–92. https://doi.org/10.37934/cfdl.17.6.8192

[30] Arafat, M., Ishak, I. A., & Mohd Maruai, N. (2024). Assessment of computational fluid dynamics simulation approach for the aerodynamic performance of small unmanned aerial vehicle propeller. *Engineering Research Express*, *6*(4). https://doi.org/10.1088/2631-8695/ad9e6c